Electric Field Modulation of Galvanomagnetic Properties of Mesoscopic Graphite

Yuanbo Zhang, Joshua P. Small, Michael E. S. Amori, and Philip Kim
Department of Physics and the Columbia Nanoscale Science and Engineering Center, Columbia University, New York, New York 10027, USA
(Received 31 August 2004; published 3 May 2005)

Electric field effect devices based on mesoscopic graphite are fabricated for galvanomagnetic measurements. Strong modulation of magnetoresistance and Hall resistance as a function of the gate voltage is observed as the sample thickness approaches the screening length. Electric field dependent Landau level formation is detected from Shubnikov–de Haas oscillations. The effective mass of electron and hole carriers has been measured from the temperature dependent behavior of these oscillations.

DOI: 10.1103/PhysRevLett.94.176803 PACS numbers: 73.63.−b, 73.22.−f, 73.23.−b

Graphite is a semimetal with a highly anisotropic electronic structure featuring nearly compensated low density electrons and holes with a very small effective mass [1]. Such an unusual electronic structure is the basis of the unique electronic properties of other graphitic materials, such as fullerenes and carbon nanotubes [2], and may lead to novel manifestations in two-dimensional graphene materials. For this reason, electron transport in graphite has recently been the subject of extensive theoretical [3,4] and experimental [5–9] investigations. In particular, interesting size dependent galvanomagnetic effects have been observed [10,11] in thin layers of graphite, with thickness approaching ~10 nm. On this mesoscopic length scale, the electrostatic-field-effect (EFE) modulation of the charge carrier concentration is expected to be very effective, owing to the low density of nearly compensated carriers in graphite.

In this Letter, we present results from the EFE dependent magnetoresistance (MR) and Hall resistance measurements in mesoscopic graphite crystallites consisting of as few as ~35 atomic layers. The mesoscopic graphite devices used in this experiment are fabricated using a unique micro-mechanical method. The details of the device fabrication are described elsewhere [12]. In brief, very thin layers of graphite crystallites with lateral size ~2 μm and thickness d ranging from 10–100 nm are extracted from bulk highly oriented pyrolytic graphite (HOPG) [13] and deposited onto SiO_2/Si substrate using micromechanical manipulations. Multiple metal electrodes (Cr/Au) are then fabricated on the corners, using electron beam lithography (Fig. 1 inset). The lateral size of the samples and electrodes are chosen so that the contribution from the graphene edge state [14] is minimal. The degenerately doped silicon substrate serves as a gate electrode with thermally grown silicon oxide (500 nm) acting as the gate dielectric.

Figure 1 displays the Hall resistance (R_{xy}) and the magnetoresistance (R_{xx}) as a function of applied magnetic field, B, measured in a 12 nm thick graphite sample at temperature $T = 1.7$ K. The excitation current is kept at 0.5 μA for both R_{xy} and R_{xx} measurements. The magnetic field is applied perpendicularly to the graphite basal plane. Both quantities exhibit oscillatory features on top of smooth backgrounds as B varies. Near $V_g \approx 0$ V, the MR and Hall resistance exhibit similar behavior to that observed in high quality bulk graphite [15]: the positive MR background is ascribed to the general nature of magnetotransport in materials with coexisting nearly compen-

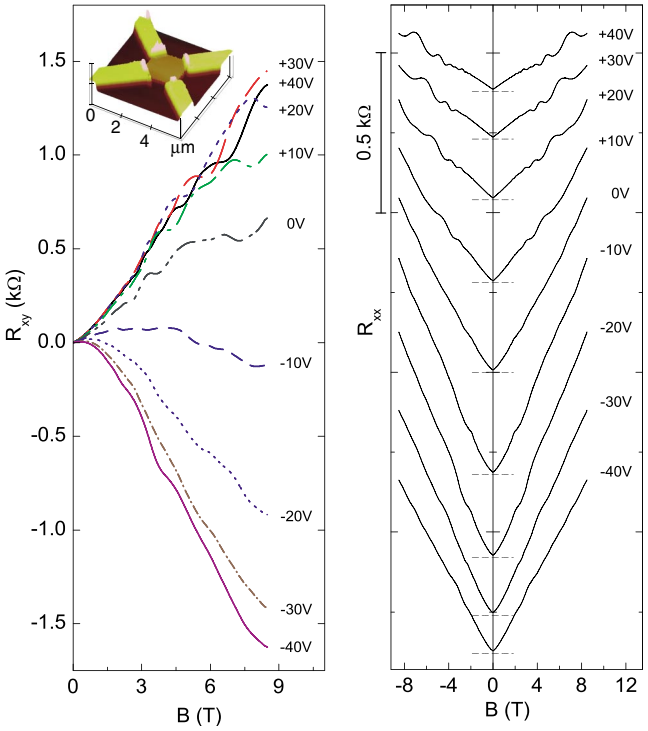

FIG. 1 (color online). The inset shows an atomic force microscope image of a 12 nm thick mesoscopic graphite sample with four electrodes. The left and right panel show the R_{xy} and R_{xx}, respectively, as a function of magnetic field measured at $T = 1.7$ K in this device. Numbers near each curve indicate the applied gate voltages. R_{xx} curves are shifted for clarity and the dashed lines correspond to the zero lines of each curve.

sated electron and hole carriers [16], while the oscillations on top of the background are related to the Shubnikov–de Hass (SdH) effect, the quantum oscillations due to Landau level formation. Remarkably, as we vary the gate voltage, V_g, the behavior of R_{xx} and R_{xy} changes dramatically. The background in the MR is most prominent at $V_g^{\max} \approx -15$ V. As V_g moves away from this value, the slope of the MR background becomes much smaller. The change of Hall measurement is even more drastic: $R_{xy}(B)$ changes its sign of overall slope as $\Delta V_g = V_g - V_g^{\max}$ swings from negative to positive values, indicating that ΔV_g changes the dominant majority charge carriers from holes to electrons. This is a somewhat surprising result at first sight, since the thickness of the sample (12 nm) is still an order of magnitude larger than the screening length of graphite ($\lambda_s \approx 0.4$ nm [17]), and thus only a relatively small portion of the sample is affected by the gate electric field. We will discuss this point quantitatively below.

The aforementioned EFE in mesoscopic graphite samples is clearly presented by observing R_{xx} as a function of gate voltage at a fixed magnetic field. Figure 2 shows R_{xx} as a function of V_g at a large magnetic field ($B_m = 8.5$ T) for two samples ($d = 12$ and 42 nm). As expected from Fig. 1, R_{xx} has a peak near a gate voltage where $\Delta V_g \approx 0$, falling slowly as $|\Delta V_g|$ becomes large. We found that this gate dependence strongly depends on d. For the 12 nm sample, R_{xx} is suppressed to ~10% of its peak value, while it is still ~60% for the 42 nm sample at $\Delta V_g = 80$ V. Such

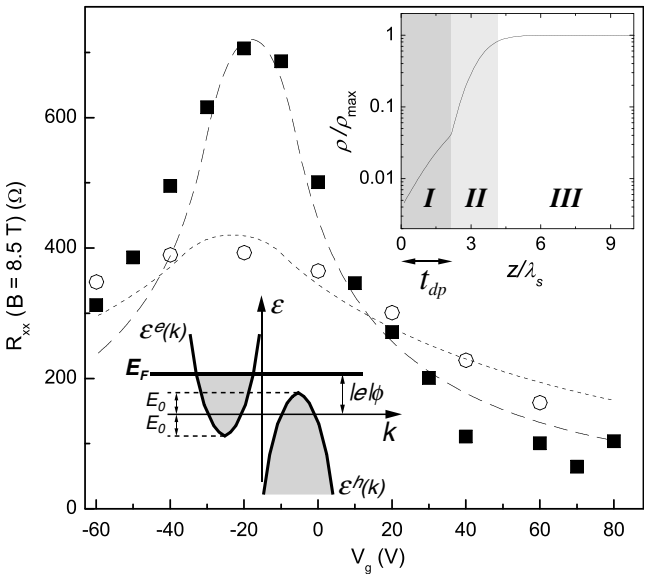

FIG. 2. R_{xx} in 12 nm (solid square) and 42 nm (open circle) thick sample at various gate voltages. The dashed and dotted lines are fits to a model described in text. The lower inset shows a schematic STB diagram for electron ($\varepsilon^e(k)$) and hole ($\varepsilon^h(k)$) in the presence of gate-induced electrostatic potential. Upper inset represents the local magnetoresistivity across the sample, assuming $\phi_0 = 8E_0/|e|$ as an example. Symbols are defined in text.

a sensitive dependence of $R_{xx}(V_g)|_{B_m}$ on d is indicative of the reduced EFE by screening of induced charge near the sample surface.

In order to elucidate the dependence of R_{xx} on V_g, we employ the simple two band (STB) model [18], which has been successful in understanding MR in graphite [6,7]. The STB model assumes that the bottom of the electron band and the top of the hole band overlap with a small band overlap $2E_0$ near the Fermi energy E_F. The resistivity of a sample, ρ, in the presence of a magnetic field can be expressed by [16]:

$$\frac{\Delta\rho}{\rho_0} = \frac{4\mu^2 B^2 n_e n_h/(n_e + n_h)^2}{1 + [\mu B(n_e - n_h)/(n_e + n_h)]^2}, \qquad (1)$$

where $\rho_0 = \rho(B = 0)$, $\Delta\rho = \rho(B) - \rho_0$, μ is the average carrier mobility, and n_e and n_h are the carrier concentrations of electrons and holes, respectively. Generally, $\Delta\rho$ varies the most as a function of B when electrons and holes are nearly compensated (i.e., $n_e \approx n_h$). From Fig. 2, we infer that this condition is met at $V_g \approx V_g^{\max}$ where the growth of the MR background as a function of B is strongest in our samples (see the curves for $V_g = -10$ V and $V_g = -20$ V in Fig. 1) [19]. As ΔV_g increases from zero, the induced charge in the sample screens the gate electric field and the electrostatic potential in the sample is given by $\phi(z) = \phi_0 e^{-z/\lambda_s}$, where z is measured from the interface between the sample and the substrate. The constant ϕ_0 can be determined from the electrostatic gate coupling to the sample. By integrating over the induced charge in the sample, we obtain $\phi_0 = \alpha\Delta V_g$ with the constant $\alpha^{-1} = 1 + \varepsilon_0(1 - e^{-d/\lambda_s})/\lambda_s C_g$, where C_g is the gate capacitance per unit area of the sample and ε_0 is the vacuum permittivity [20].

We incorporate this local electrostatic potential to the STB model by considering a gradient in n_e and n_h. Suppose $\Delta V_g > 0$, the local electrostatic potential will pull down the electron and hole bands by $|e|\phi(z)$ (Fig. 2 lower inset). For a sufficiently large gate voltage, such that $|e|\phi_0 > E_0$, the sample can be divided into three regions by introducing a hole depletion depth, $t_{dp} = \lambda_s \log(|e|\phi_0/E_0)$: (I) $0 < z < t_{dp}$, where $n_h \simeq 0$; (II) $t_{dp} < z \lesssim t_{dp} + \lambda_s$, where $0 < n_h < n_e$; and (III) $z > t_{dp} + \lambda_s$, where $n_h \approx n_e$. In region (I), only electrons participate in the transport, and $\rho(z)$ increases as z approaches zero, owing to the electric field induced accumulation of n_e near the surface. In region (II), the MR is described by Eq. (1), so a steep increase of $\rho(z)$ is expected as $n_e - n_h$ becomes small. In region (III), the gate electric field is completely screened, so $n_e \approx n_h$ and $\rho(z) \approx \rho_{\max} = R_{xx}(\Delta V_g = 0)d$. The exact opposite argument works for a sufficiently large negative gate voltage, where electrons are depleted. Note that for small $|\Delta V_g|$, where $|e\phi_0| < E_0$, region (I) disappears (i.e., $t_{dp} = 0$). From the above discussion, we now build a quantitative model to describe

$\rho(z)$. According to the STB model $n_e(\epsilon)$, $n_h(\epsilon) \propto \epsilon^{3/2}$, where ϵ is measured from the bottom of the respective band edge, and $\rho(z)/\rho_{\max}$ is obtained from Eq. (1) (Fig. 2 upper inset). Then the resistance of the sample can be evaluated from $R_{xx}^{-1} = \int_0^d \rho^{-1}(z)dz$ for fixed B and V_g. Following in this way, a reasonable fit is obtained for both the 12 nm (dashed line) and 42 nm (dotted line) samples as shown in Fig. 2. In this fit, we use $E_0 =$ 15 meV, a value quoted in [1], and obtain $C_g =$ 26 aF/μm^2 (12 nm sample) and 24 aF/μm^2 (42 nm sample) as a result of the fit. These capacitance values are in reasonable agreement with our previous estimates using different analysis on the same samples [12]. It is noteworthy that for a large V_g such that $|e|\phi_0 \gg E_0$, $\rho(z) \ll \rho_{\max}$ in region (I), and thus a significant portion of the total current flows in this region. Furthermore, as ΔV_g increases, t_{dp} grows only logarithmically. Even at $\Delta V_g \approx 100$ V, the largest gate voltage applied, $t_{dp} \approx 1$ nm, which corresponds to only $\sim$3 bottom layers. Therefore, only a few of the bottom layers of the sample are responsible for the observed EFE modulation of the galvanomagnetic transport quantities.

We now turn our attention to the quantum oscillations observed in our mesoscopic graphite samples. The strong EFE modulation of the carrier density in the bottom layers allows us to probe the quantum oscillations in these layers with a continuously tunable carrier concentration. The estimated mobility and carrier density from our measurement in the nearly compensated region are $\mu_{e,h} \sim$ 50 000 cm^2/V sec and $n_e \approx n_h \sim 10^{18}$ cm^{-3} at 1.7 K. Figure 3(a) redisplays the separated SdH oscillations as a function of B^{-1}, obtained from the MR data shown in Fig. 1 after subtracting out the smooth background. The SdH oscillations indicate the oscillatory density of states at E_F as a quantized Landau level passes through E_F. The frequency of SdH oscillations, f_s, is related to the extremal area of the electron and hole pockets of the Fermi surface by $f_s = \hbar c A_k^{e,h}/2\pi|e|$, where A_k^e and A_k^h are the areas of extremal electron and hole pockets [21], and $\hbar$ and c are Planck's constant and the speed of light, respectively. Since n_e and n_h are modulated by V_g, the observed variation of f_s can be explained by the change of $A_k^{e,h}$.

In order to demonstrate the change of f_s quantitatively, we first locate the major peaks (solid symbols) and valleys (open symbols) in the SdH oscillations after low pass filtering of the data [22]. The value of B^{-1} for a peak (valley), B_m^{-1}, is indexed by ν, an integer (a half integer) number that corresponds to the Landau level responsible for the particular oscillation. Figure 3(b) shows that each set of points (B_m^{-1}, ν) at a given V_g are on a straight line that intercepts the origin, implying that the period of the SdH oscillations is regular. From the slope of these lines we obtain f_s at different V_g [Fig. 3(b)]. The obtained f_s's are increasing with $|\Delta V_g|$. Therefore, we believe that the

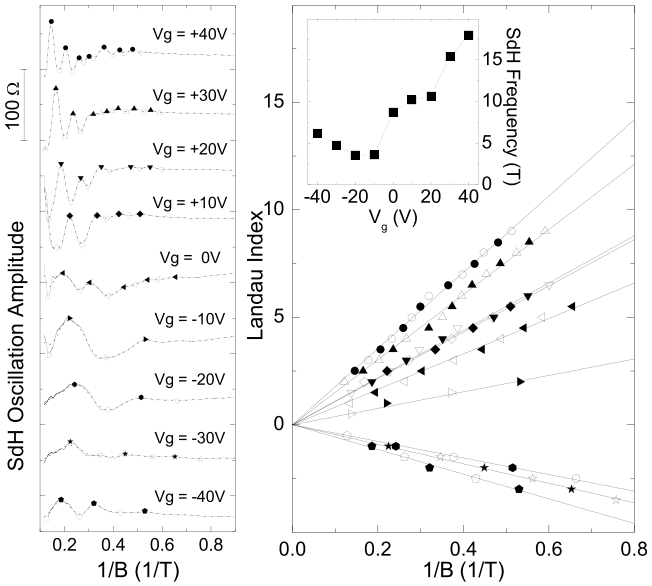

FIG. 3. (a) The SdH oscillations observed in Fig. 1, after subtraction of smooth backgrounds. Solid (open) symbols correspond to peak (valley) of the oscillations found after passing the curve through a low pass filter (dotted line). Curves are displaced for clarity. (b) Landau plots (see text) obtained from (a). Lines are linear fits to each set of points at different V_g. Inset: the frequency of the SdH oscillations obtained from the slopes of the line fits in (b) at different V_g.

obtained f_s corresponds to A_k^e for $\Delta V_g > 0$ and to A_k^h for $\Delta V_g < 0$. This conclusion allows us to compare the experimentally observed f_s with the expected value from the STB model. Assuming the Fermi surface of graphite is described by the overlap of electron and hole bands in the STB model, $A_k^e \propto (\alpha \Delta V_g + E_0)$ and $A_k^h \propto (-\alpha \Delta V_g + E_0)$. This relationship leads to $f_s(|\Delta V_g|)/f_s^0 = 1 + \alpha|\Delta V_g|/E_0$, where $f_s^0 = f_s(\Delta V_g = 0)$. From the values of α and E_0, determined separately above, we estimate $f(\Delta V_g = 50\ \text{V})/f_0 \approx 4.8$, which is in reasonable agreement with the experimentally observed ratio 4.3.

Finally, we discuss the temperature dependence of the SdH oscillations. Figure 4 shows the oscillatory MR at two extreme gate voltages, $V_g = +40$ V and $V_g = -60$ V, at various temperatures. At these extreme gate voltages, the transport in the sample is dominated by only one type of carrier in a few bottom layers. Thus, the SdH oscillations in the upper (lower) panel of the figure correspond to electron (hole) Landau levels in the sample. In both cases, the observed SdH oscillation amplitude is gradually damped away as the temperature increases. The temperature dependent SdH oscillation amplitude has been used to extract the effective mass of the charge carriers [23]. At a fixed magnetic field, the temperature damping factor of the SdH oscillation amplitude is proportional to $\pi k_B T m^*/ehB \sinh(\pi k_B T m^*/ehB)$, where m^* is the effective mass of the carriers. We find that this function fits the

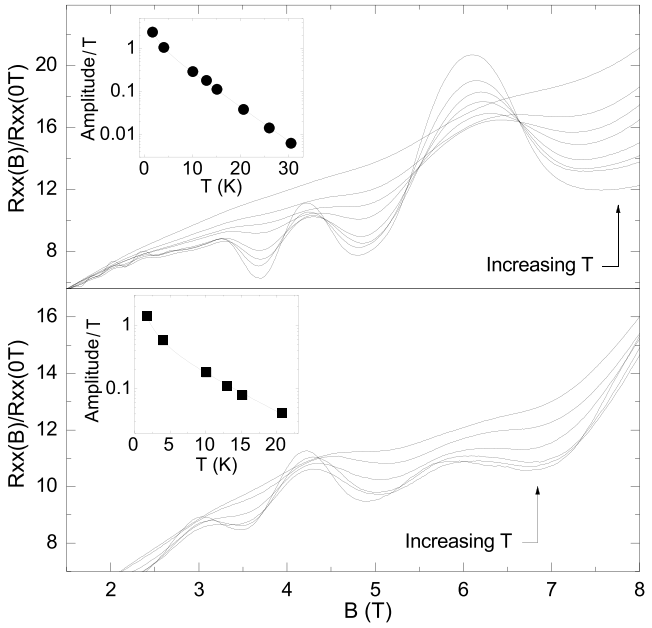

FIG. 4. Normalized magnetoresistance of the sample in Fig. 1 at $V_g = 40$ V (upper panel) and $V_g = -60$ V (lower panel). Data are taken at temperatures 1.7, 4, 10, 13, 15, 20, 25, and 30 K. Insets: SdH oscillation amplitudes divided by temperature, T, at a fixed magnetic field. The solid lines are fits to a model (see text).

observed amplitude damping very well (Fig. 4 insets). As a result from the fittings, the effective electron mass $m_e^* = (0.052 \pm 0.002)m_e$ and hole mass $m_h^* = (0.038 \pm 0.002)m_e$ are obtained, where m_e is the bare electron mass. While the hole mass in this sample agrees well with the reported value of the hole mass ($0.039m_e$) in a high quality bulk graphite crystal [1], m_e^* shows a $\sim$10% reduction from the corresponding bulk value ($0.057m_e$), suggesting potential band structure modifications in the mesoscopic samples.

In summary, we report strong modulation of the Hall resistance and the magnetoresistance in mesoscopic graphite samples consisting of tens of graphene layers as a function of applied gate voltage. These phenomena have not been observed in bulk samples [24]. The electric field effect changes the sign of the dominant majority carrier, hence reverses the sign of the Hall coefficient. The Landau level formation of electron and hole carriers is also tuned by the electric field effect.

We thank H. L. Stormer, A. Millis, and I. Aleiner for helpful discussions. This work is supported primarily by the Nanoscale Science and Engineering Initiative of the National Science Foundation under NSF Grant No. CHE-0117752 and by the New York State Office of Science, Technology, and Academic Research (NYSTAR).

Note added.—During the preparation of this manuscript, we became aware of related work on similar systems from other groups [25].

[1] N. B. Brandt, S. M. Chudinov, and Y. G. Ponomarev, *Semimetals 1: Graphite and Its Compunds* (North-Holland, Amsterdam, 1988).
[2] M. S. Dresselhaus, G. Dresselhaus, and P. C. Eklund, *Science of Fullerenes and Carbon Nanotubes* (Academic, New York, 1996).
[3] D. V. Khveshchenko, Phys. Rev. Lett. **87**, 206401 (2001); **87**, 246802 (2001).
[4] C. D. Spataru, M. A. Cazalilla, A. Rubio, L. X. Benedict, P. M. Echenique, and S. G. Louie, Phys. Rev. Lett. **87**, 246405 (2001).
[5] Y. Kopelevich, J. H. S. Torres, R. R. daSilva, F. Mrowka, H. Kempa, and P. Esquinazi, Phys. Rev. Lett. **90**, 156402 (2003).
[6] T. Tokumoto, E. Jobiliong, E. S. Choi, Y. Oshima, and J. S. Brooks, Solid State Commun. **129**, 599 (2004).
[7] X. Du, S. Tsai, D. L. Maslov, and A. F. Hebard, cond-mat/0404725.
[8] L. M. Viculis, J. J. Jack, and R. B. Kaner, Science **299**, 1361 (2003).
[9] X. Lu, H. Huang, N. Nemchuk, and R. Ruoff, Appl. Phys. Lett. **75**, 193 (1999); X. Lu, M. Yu, H. Huang, and R. Ruoff, Nanotechnology **10**, 269 (1999).
[10] E. Dujardin, T. Thio, H. Lezec, and T. W. Ebbesen, Appl. Phys. Lett. **79**, 2474 (2001).
[11] Y. Ohashi, T. Hironaka, T. Kubo, and K. Shiiki, Tanso **1997**, 235 (1997); **2000**, 410 (2000).
[12] Y. Zhang, J. P. Small, W. V. Pontius, and P. Kim, Appl. Phys. Lett. **86**, 073104 (2005).
[13] HOPG Grade-1, Structure Probe, Inc.
[14] K. Nakada, M. Fujita, G. Dresselhaus, and M. S. Dresselhaus, Phys. Rev. B **54**, 17954 (1996).
[15] D. E. Soule, Phys. Rev. **112**, 698 (1958).
[16] I. L. Spain, Carbon **17**, 209 (1979).
[17] P. R. Visscher and L. M. Falicov, Phys. Rev. B **3**, 2541 (1971).
[18] For an extensive summary see, for example, B. T. Kelly, *Physics of Graphite* (Applied Science, London, 1981), p. 285.
[19] The STB model is too simplified to describe transport in the low field regime where $\Delta R_{xx}(H)/R_{xx}$ increases rather linearly than quadratic increase. In order to capture a full description of Fermi surface, a more detailed model is required.
[20] We estimate the change of λ_s is less than 10% even at the highest applied V_g, and neglect this effect in our model.
[21] Within the STB model, the Fermi surface anisotropy is simply ignored.
[22] Because of the strong positive MR background, we choose only dominant high frequency SdH oscillations for our analysis.
[23] D. Shoenberg, *Magnetic Oscillations in Metals* (Cambridge University Press, Cambridge, England, 1984).
[24] H. Kempa and P. Esquinazi, cond-mat/0304105.
[25] K. S. Novoselov *et al.*, Science **306**, 666 (2004); J. S. Bunch *et al.*, Nano Lett. **5**, 287 (2005); C. Berger *et al.*, J. Phys. Chem. B **108**, 19912 (2004).